

Foam Mobility Control for Surfactant Enhanced Oil Recovery

Robert Feng Li, SPE, Rice University; Wei Yan, SPE, IPSI; Shunhua Liu, SPE, Occidental Oil and Gas; and George J. Hirasaki, SPE, and Clarence A. Miller, SPE, Rice University

Summary

Foam generated in situ by surfactant-alternating-gas (SAG) injection is demonstrated as a substitute for polymer drive in the alkaline/surfactant/polymer (ASP) enhanced-oil-recovery (EOR) process. Foam is also effective in a similar process for a 266-cp crude oil, even though the system did not have enough polymer for favorable mobility control. Foam is shown to enhance sweep efficiency greatly in a layered sandpack with a 19:1 permeability ratio. Foam diverted surfactant solution from the high-permeability layer to the low-permeability layer. Ahead of the foam front, liquid in the low-permeability layer crossflowed into the high-permeability layer. A layered system with a 19:1 permeability contrast could be completely swept in 1.3 total pore volumes (TPV) with foam, while waterflood required 8 pore volumes (PV).

Introduction

Foam as a means for mobility control of surfactant flooding was introduced 28 years ago by Lawson and Reisberg (1980). This concept was not adopted immediately because of the lack of understanding of the mechanism of mobility control with foam. Since that time, there have been many advances in the understanding of foam mobility control. There have been many field tests of steam foam (Hirasaki 1989; Patzek 1996) and CO₂ foam. One of the most successful field demonstrations of foam mobility control was in the Snorre field (Blaker et al. 2002). Foam was used as mobility control for surfactant aquifer remediation at Hill Air Force Base in Utah (Hirasaki et al. 1997, 2000). Foam was used as mobility control for alkaline surfactant flooding in China (Zhang et al. 2000; Wang et al. 2001).

The most important advance in understanding that has made foam mobility control practical is the understanding of the condition necessary to generate strong foam. There is a critical pressure gradient that must be exceeded to generate strong foam during the flow of surfactant solution and gas through homogeneous porous media (Falls et al. 1988; Gauglitz et al. 2002; Kam and Rossen 2003; Rossen 1996; Rossen and Bruining 2007; Tanzil 2002b). Below this pressure gradient, gas may flow as a continuous phase with only modest mobility reduction. Above this pressure gradient, stationary bubbles are mobilized such that bubble trains have multiple branch points. A flowing bubble divides into two bubbles at each branch point and thus regenerates bubbles that are lost to coalescence. Foam bubbles can also be regenerated (independent of pressure gradient) when gas and surfactant solution flow across a step increase in permeability with a ratio greater than 4 (Falls et al. 1988; Tanzil et al. 2002a). If one recognizes the critical pressure gradient necessary for strong foam, experiments can be conducted at high enough flow rate or pressure drop such that the critical pressure gradient is exceeded.

The other important advance in understanding is the observation that, when the foam is flowing with conditions where it is regenerated in situ, the gas mobility is determined by a limiting capillary pressure, above which the lamellae become unstable and bubbles coalesce (Khatib et al. 1988). This understanding explains why, in this regime, the pressure gradient is a function of the liquid-flow rate but is independent of the gas-flow rate. Also, foam

mobility can be modeled by fractional-flow theory in this flow regime (Gauglitz et al. 2002; Rossen 1996). In this regime, gas mobility increases with increasing gas fractional flow and decreasing permeability. This permeability dependence makes foam especially useful for improving sweep in layered systems (Heller 1994; Bertin et al. 1999; Kovscek and Bertin 2002). The dependence of foam mobility on fracture aperture has been demonstrated to be beneficial in the sweep of fracture systems (Yan et al. 2006). Foam propagation in layered flow models with permeability contrast has been investigated with and without crossflow (Bertin et al. 1999; Nguyen et al. 2005) and in foam-induced acid diversion (Gdanski 1993; Zhou and Rossen 1994). In a layered system where capillary communication is allowed and crossflow is present, foam propagates almost simultaneously in both high- and low-permeability layers; whereas, in a system with isolated layers where capillary communication is prohibited, foam forms in the high-permeability layer and diverts foam to the low-permeability layer, resulting in a faster advancing foam front in the low-permeability layer.

It is generally recognized that oil tends to destabilize foam. However, the amount of destabilization depends on oil-, surfactant-, and aqueous-phase compositions. To destabilize a foam lamella, an oil drop must first overcome electrostatic or steric interactions in the aqueous pseudoemulsion film, which forms as the drop approaches the gas/water interface (Nikolov et al. 1986; Manlowe and Radke 1990). Then, provided that the aqueous phase does not spread at the gas/oil interface so formed, the oil forms a lens that can destabilize the lamella by spreading along the gas/water interface (Lau and O'Brien 1988), by bridging (Garrett 1992), or by some combination of the two. It is a common observation during phase behavior of oil/water/surfactant systems that foam is more stable with Winsor I phase behavior and more unstable with Winsor II or III phase behavior.

The high apparent viscosity shown here raises questions about its effect on injectivity. However, foam is a shear-thinning fluid, and this effect should be included when calculating injectivity (Li et al. 2006).

Here, we show that foam generated in situ by SAG injection can replace the polymer drive in ASP EOR. Foam is also effective as an ASP process for a 266-cp crude oil, even though the system did not have enough polymer for favorable mobility control. We also show and discuss the mechanisms of how SAG increases sweep efficiency in a 2D horizontal model having two sand layers with a significant permeability contrast.

Experimental Procedure

Materials. Three surfactants or their blends were used in this investigation:

- AOS 16-18 (sodium 16-18 alpha olefin sulfonate, Stepan)
- IOS 15-18 (sodium 15-18 internal olefin sulfonate, Shell)
- Neodol 67-7PO (ammonium C16-17 7PO sulfate, Stepan)
- NI Blend is a blend of 4:1 (wt/wt) Neodol 67-7PO and IOS 15-18.
- Flopaam 3330S (SNF Floerger) is a partially hydrolyzed polyacrylamide, $M_w \approx 8 \times 10^6$.

Three crude oils were used:

- MY: Yates, west Texas [19 cp at 25°C, total acid number (TAN) = 0.75 mg KOH/g]
- SMY: Deepwater Gulf of Mexico (15 cp at 25°C, TAN = 0.34 mg KOH/g)
- Crude B: viscous oil (266 cp at 25°C, TAN = 4.8 mg KOH/g)

Copyright © 2010 Society of Petroleum Engineers

This paper (SPE 113910) was accepted for presentation at the SPE/DOE Symposium on Improved Oil Recovery, Tulsa, 20–23 April 2008, and revised for publication. Original manuscript received for review 12 February 2008. Revised manuscript received for review 24 November 2009. Paper peer approved 1 March 2010.



Fig. 1—Photograph of 2D heterogeneous sandpack. Arrows show direction of flow through manifolds.

Three silica sands from U.S. Silica Company were used:

- Oil Frac 20/40 (79–200 darcies)
- F-42 (40 darcies)
- F-110 (4.8 darcies)

Na_2CO_3 (anhydrous, certified American Chemical Society) and NaCl (biological certified) were both obtained from Fisher Scientific.

Green dye was made of 3 mL green food coloring (water, propylene glycol, yellow dye number 5, blue dye number 1, brand name McCormick, purchased from Kroger) dissolved in 1000 mL of brine.

Equipment

1D Homogeneous Sandpack. The 1D system was a 1-ft-long glass column with 1-in. inner diameter packed with silica sand. All columns were dry packed and were tightly packed by continuously tapping the glass wall during packing to induce mixing and settling. Each end was sealed by a rubber stopper, and a metal screen was put between the rubber and the sand. A high-pressure liquid chromatography (HPLC) pump (ISCO Model 2350) and a syringe pump (Harvard Apparatus) were used for fluid injection. Pressure was measured and recorded by a pressure transducer (Validyne, Northridge) connected to a computer. The ASP foam experiments were conducted with vertical, upward flow. For constant-rate injection, liquid was injected by an HPLC pump and gas (air) was injected by a syringe pump specified at a certain volumetric-flow rate. For constant-pressure injection, liquid and gas were injected manually by monitoring the pressure so that it was maintained within $\pm 10\%$ of the specified value. Liquid and gas rates reported for constant-pressure injection were averaged values of slug volume divided by injection time. All experiments were conducted at ambient room temperature.

2D Heterogeneous Sandpack. The 2D system is made of stainless steel with a glass observation window 1.25 in. thick in the front (donated by Shell). The interior is a $20 \times 3 \times 0.75$ -in. chamber (Fig. 1). There are 21 ports with 60- and 200-mesh screens: three on the left, three on the right, and 15 at the back. The pressure ports are designed for pressure measurement during the flow experiment. These inner pressure taps help overcome end-piece effects that could result in extra pressure drop.

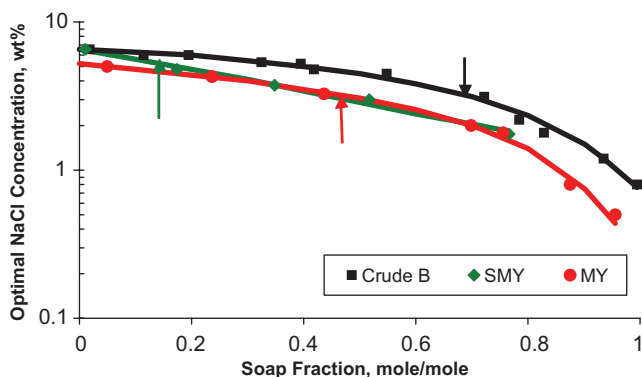


Fig. 2—Phase behavior of MY, SMY, and Crude B with NI blend.

The model was packed with two layers of silica sand, Oil Frac 20/40 on top and F-110 on bottom. Of the top and bottom layers, the thickness ratio was 2:3 and the permeability ratio was 19:1 (90 and 4.8 darcies). The TPV was 332.1 mL. The overall porosity was 0.381, and the measured overall permeability was 38.5 darcies. Overall permeability was measured by injecting water through a manifold, as shown in Fig. 1. Pressure drop across the entire sandpack was measured. Overall permeability was then calculated using Darcy's law. It should be noted that the arithmetic-average value of upper and lower permeabilities, taking into account the thickness ratio, agreed very well with the measured overall 2D permeability. The calculated arithmetic-average permeability was 38.4 darcies. The measured overall 2D permeability was 38.5 darcies by constant-rate injection or 34.5 darcies by constant-pressure injection. Fig. 1 is a photograph of the sandpack saturated with water.

Results and Discussion

Phase Behavior of Crude Oils With NI Blend. The phase behavior of the NI blend of surfactants with different crude oils was investigated at room temperature. All systems had 1% Na_2CO_3 . Salinity scans with increasing NaCl were conducted to determine the optimal salinity, expressed as wt% NaCl . Optimal salinities were estimated on the basis of trends in solubilization and changes in color of the aqueous phase when the surfactant became preferentially oil soluble. Quantitative solubilization ratios could not be used to confirm these estimates because either surfactant concentration was too low or the phases were too dark (for Crude B) to measure these ratios. The optimal salinities for the three crude oils and NI blend are shown in Fig. 2 as a function of the fraction soap/(soap+surfactant), with soap content based on the amount of soap extracted from the crude oil for highly alkaline conditions as measured by aqueous-phase titration (Liu et al. 2008a). Arrows in this figure show the values of the soap fraction determined from the water/oil ratio corresponding to waterflood residual-oil saturation.

While it may appear favorable to inject the surfactant solution at the optimal salinity for minimum interfacial tension (IFT), mobility control will be lost if the surfactant slug separates into surfactant-rich and polymer-rich phases (Liu et al. 2008b). Previous sandpack experiments (Liu et al. 2008b) showed that, when the salinity was 4% NaCl such that polymer and surfactant separated into different phases, poor sweep and high pressure gradients resulted. Thus, injection compositions were designed such that the surfactant and polymer remained as a single, clear phase. The ASP slugs discussed later were injected at 2% NaCl for the MY and SMY crude oils and at 1% NaCl for Crude B. A lower injected salinity was used for the Crude B because the high acid number for this crude oil generated much more soap than the other crude oils. This formulation reduced oil/water IFT to the order of 10^{-3} mN/m and had displaced oil successfully in previous ASP sandpack experiments (Liu et al. 2008b). Simulations indicate that high recovery is possible for a wide range of conditions with injection below optimal salinity of the surfactant owing to development of a gradient in soap fraction (Liu et al. 2008a).

Foam for Mobility Control of ASP Process in 40- and 200-darcy Sandpacks. The performance of ASP flood with foam mobility control (ASPF) and MY crude oil was compared in 40- and 200-darcy silica sandpacks. The initial conditions for the ASPF

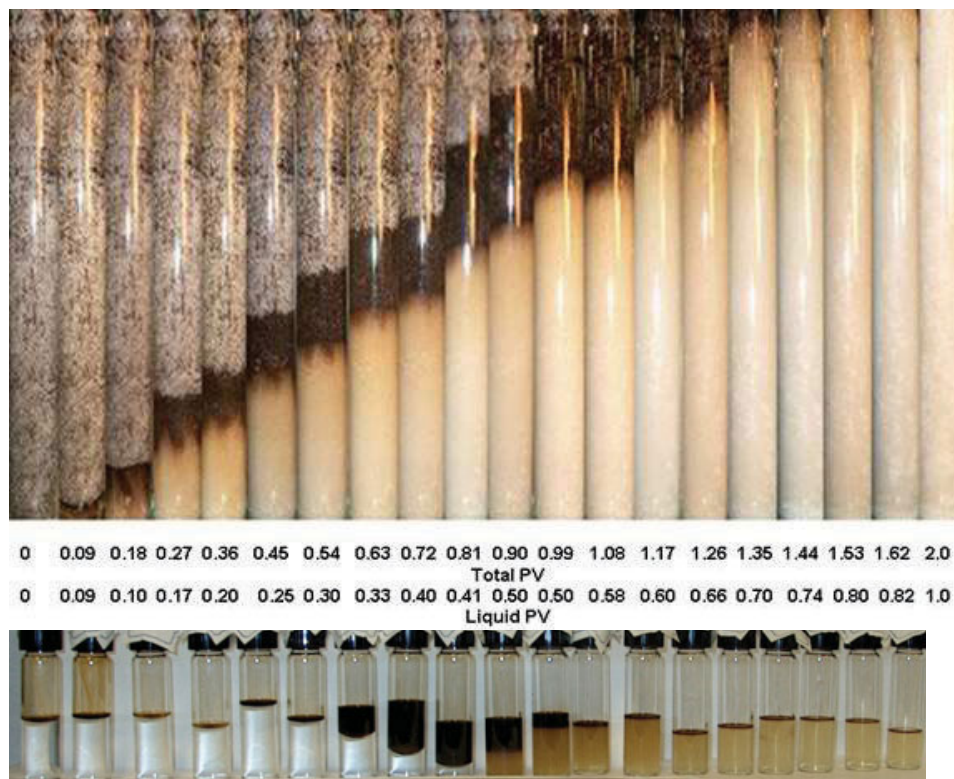


Fig. 3—Displacement profiles and pictures of effluent for the displacement of MY residual crude oil by ASPF in 40-darcy sandpack.

were waterflood residual-oil saturation of 25% and 30% in the 40- and 200-darcy packs, respectively. (The latter may have had some emulsified oil that was not displaced by the waterflood.) The pressure drop had decreased from the beginning to the end of waterflood. At the end of waterflood, where zero oil cut was observed, pressure drop was approximately three times that of a water-saturated sandpack at the same flow rate. The brine was 2% NaCl throughout. The surfactant slug was 0.2% NI blend, 0.5% polymer, 1% Na₂CO₃, and 2% NaCl (NIP). The slug viscosity was approximately 46 cp. It was injected as 0.1-PV slugs alternating with 0.1 PV of air at a superficial velocity of 20 ft/D, for 0.6 TPV. The drive was 0.2% IOS 15-18, 1% Na₂CO₃, and 2% NaCl, injected as 0.1-PV slugs alternating with 0.1 PV of air at a superficial velocity of 20 ft/D. The injection rate was higher than in normal field operation because the sandpacks in these experiments had much higher permeability than reservoir rocks. The high rate was to ensure that the critical pressure gradient to generate strong foam was exceeded. The first step of NIP-alternating-air injection was to increase the capillary number by reducing IFT to an ultralow value and thereby reduce phase trapping. The addition of polymer was to provide mobility control in the NI blend slug. As a result of improved sweep efficiency, it was easier for foam to generate with less residual oil present because crude oil breaks foam. The next step of IOS 15-18-alternating-air injection served as a foam drive to replace polymer as mobility control. The drive used only IOS 15-18 because it was a better foaming surfactant than Neodol 67-7PO.

The displacement profiles and pictures of effluent are shown in Figs. 3 and 4 for the 40- and 200-darcy experiments, respectively. The oil recovery and apparent viscosity are shown in Figs. 5 and 6, respectively. The pressure difference is shown in Fig. 7. Oil was recovered earlier in the 200-darcy experiment. The final recovery was 94 and 96% of the waterflood remaining oil for the 40- and 200-darcy sandpacks, respectively.

If treated as single-phase flow, foam apparent viscosity in this paper was calculated from single-phase Darcy's law, $\mu_{app} = \frac{k}{uL}(P - P_{static})$, where k was the measured permeability of the sandpack, u was the superficial injection velocity, L was the

length of the sandpack, and $(P - P_{static})$ was the pressure difference across the sandpack. In Fig. 6, the apparent viscosity during liquid injection appears to be higher than that during gas injection. Injecting liquid made the system wetter (decreased foam quality), corresponding to a higher liquid-flow rate than that of gas. In the high-quality regime (Osterloh and Jante 1992), given fixed total injection rate, pressure gradient and, hence, apparent viscosity increased as a result of decreased foam quality. The contrast in the apparent viscosity between the two experiments is remarkable. The 200-darcy experiment had abnormally high apparent viscosity during the first 0.1 PV injection of ASP before any air injection. This may have been because of emulsified oil that was inadvertently introduced into the sandpack and not displaced by the waterflood (see initial conditions in Fig. 4). However, the apparent viscosity of the 200-darcy experiment remained approximately a factor of 4 to 5 higher than that of the 40-darcy experiment, even after most of the oil was displaced. This may be responsible for the faster oil recovery in the 200-darcy experiment. The pore structure in these two sandpacks was similar, and the mechanism of foam formation and resulting foam structure were similar, with the result that the relative permeability of each fluid was approximately the same in the two experiments. The apparent viscosity was then roughly proportional to permeability.

Comparison of Constant-Rate With Constant-Pressure Injection in ASPF. The performance of the ASPF process was compared when injection was by either constant rate or constant pressure. The experiment differed from those of the preceding section in that 15-cp SMY crude oil was used instead of 19-cp MY crude oil. The sandpack permeability was between 79 and 98 darcies, and the waterflood residual-oil saturation was between 23 and 26%.

The brine was 2% NaCl throughout. The surfactant slug was 0.2% NI Blend, 0.5% polymer, 1% Na₂CO₃, and 2% NaCl. The slug viscosity was approximately 47 cp. It was injected as 0.1-PV slugs alternating with 0.1 PV of air for 0.6 TPV, similar to MY experiments discussed earlier because phase behavior with NI blend of MY and SMY crudes was similar, as shown in Fig. 2. The drive was 0.5% IOS 15-18, 1% Na₂CO₃, and 2% NaCl, injected as 0.1-PV slugs alternating with 0.1 PV of air. The constant-rate

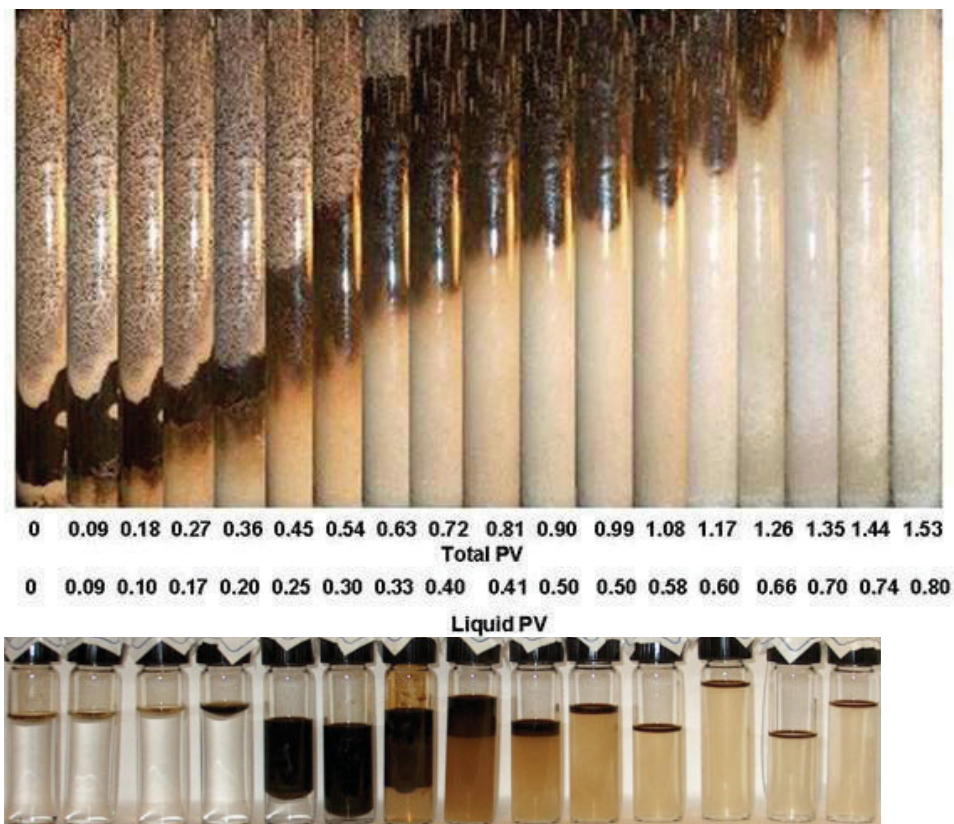


Fig. 4—Displacement profiles and pictures of effluent for the displacement of MY residual crude oil by ASPF in 200-darcy sandpack.

experiment was 20 ft/D. The constant-pressure experiment was conducted at 1.2 psi/ft.

The displacement profiles and pictures of effluent are shown in Figs. 8 and 9 for the constant-rate and constant-pressure experiments, respectively. The recovery of the SMY residual oil and apparent viscosity are shown in Figs. 10 and 11, respectively. The injection-pressure gradient is shown in Fig 12.

Comparison of the recovery curves in Fig. 10 shows that the constant-pressure experiment recovered oil earlier than the constant-rate experiment. These experiments were conducted with the expectation that a critical pressure gradient had to be exceeded to generate strong foam. First, the pressure gradient during constant-pressure injection was always higher than during the constant-rate injection. It should be noted that the maximum pressure gradient in the constant-rate experiment did not exceed 1.25 psi/ft. As a result, strong foam was generated faster with constant-pressure injection. Second, gas was more compressed during constant-pressure injection because of the higher pressure gradient. The gas expanded as

it moved through the sandpack, resulting in earlier oil recovery. Fig. 11 does not show a clear difference in foam strength (apparent viscosity) between the constant-rate and constant-pressure experiments. Apparent viscosity for the constant-pressure injection had only one data point at the end of each fluid-slug injection because only one averaged flow rate was measured during each slug injection.

The critical pressure gradient was determined from oil-free foam experiments in 1D sandpack such that there was a rapid rise in pressure drop (or apparent viscosity), as shown in Figs. 13 and 14. Generally, it was the inflection point in the pressure-vs.-PV curves. However, critical pressure gradient was chosen in a conservative manner to ensure strong foam formation for all injection velocities studied. This appears to be an upper bound, assuming only strong foam was formed. Fig. 15 showed that constant-pressure injection produced a very high injection rate at the beginning. However, the rate was reduced after foam was formed.

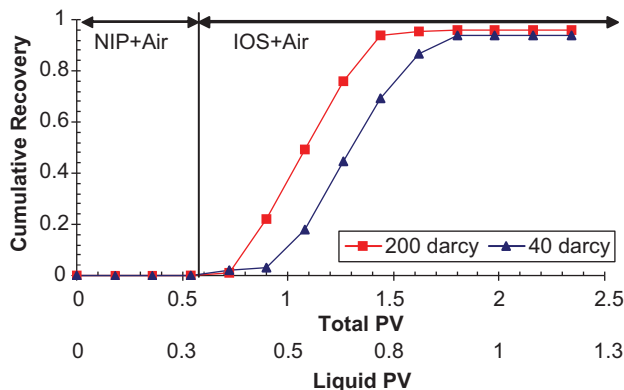


Fig. 5—Recovery efficiency for the displacement of MY residual crude oil by ASPF in 40- and 200-darcy silica sandpacks.

Displacement of Viscous (266-cp) Crude Oil by ASPF Process.

The ASPF process was used to displace Crude B, which has a viscosity of 266 cp. The remaining oil saturation was 36% after 6 PV of waterflood in a 106-darcy silica sandpack. The salinity was 1% NaCl throughout. A 0.3-PV ASP slug of 0.5% NI Blend, 0.5% polymer, 1% Na_2CO_3 , and 1% NaCl was first injected at 1 ft/D. The viscosity of this slug was approximately 46 cp. A salinity of 1% NaCl was selected because of the high acid content of this crude oil. Slugs of air (0.1 PV) were then injected, alternating with 0.1-PV slugs of NIP to 0.8 TPV at 20 ft/D. Following this, the drive consisted of 0.1-PV slugs of 0.5% IOS 15-18, 1% Na_2CO_3 , and 1% NaCl alternating with 0.1-PV slugs of air at 20 ft/D. The higher injection rate was to ensure strong-foam generation. The displacement profiles, oil recovery and oil cut, and apparent viscosity and pressure gradient are shown in Figs. 16 through 18, respectively.

The ASPF process recovered 93% of the waterflood remaining oil. The oil viscosity is 266 cp, while the surfactant slugs with 0.5% polymer (NIP) had a viscosity of approximately 46 cp. This surfactant slug had a very unfavorable viscosity ratio with respect

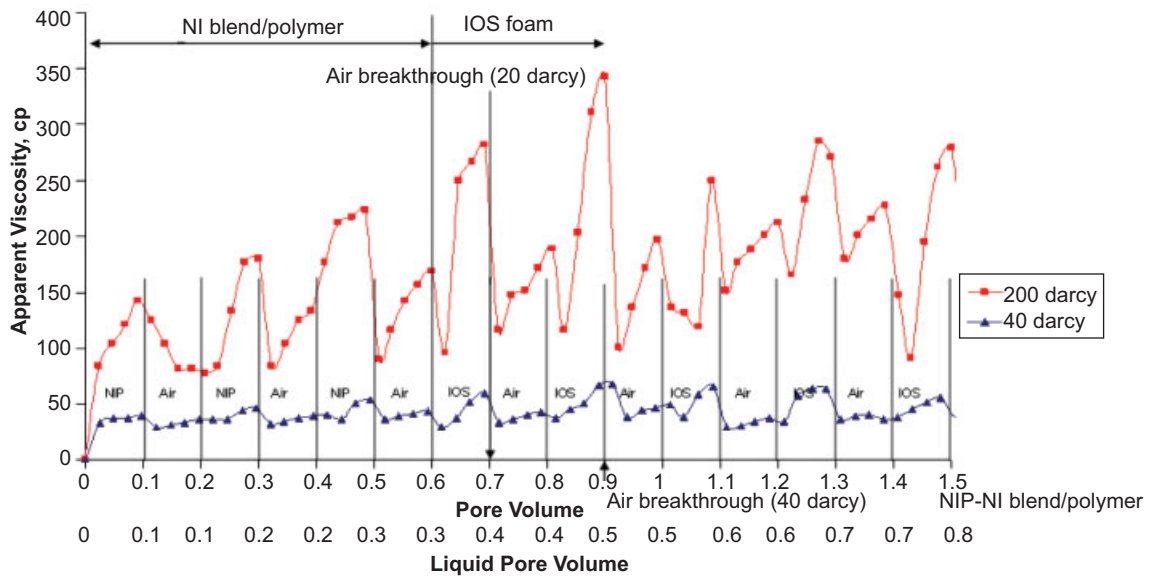


Fig. 6—Apparent viscosity during the ASPF displacing MY oil for 40- and 200-darcy sandpacks.

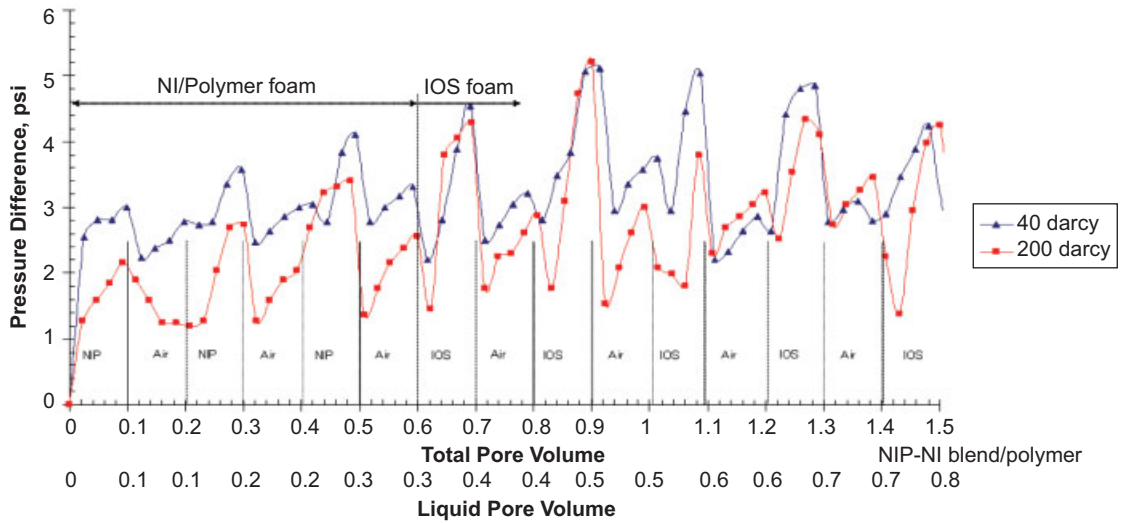


Fig. 7 —Pressure difference during the ASPF displacing MY oil for 40- and 200-darcy sandpacks.

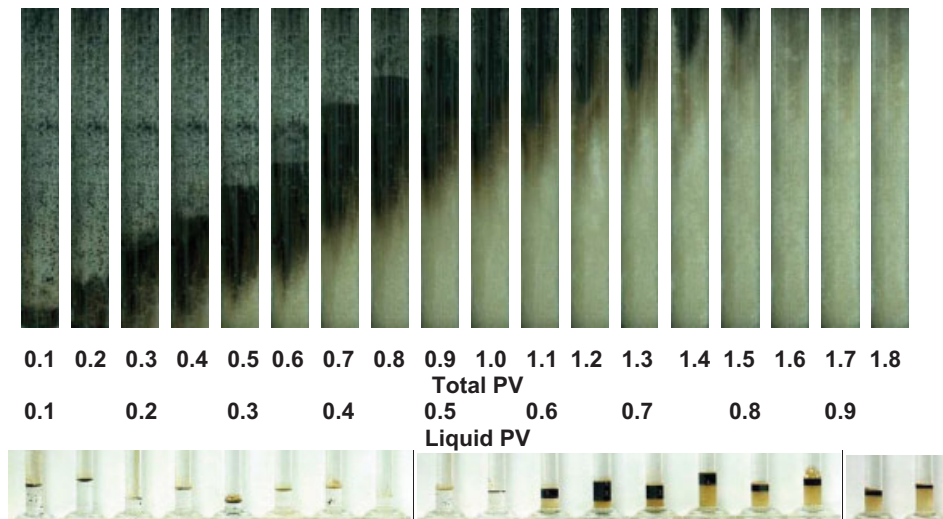


Fig. 8—Displacement profiles and pictures of effluent for the displacement of SMY residual crude oil by ASPF with constant-rate injection.

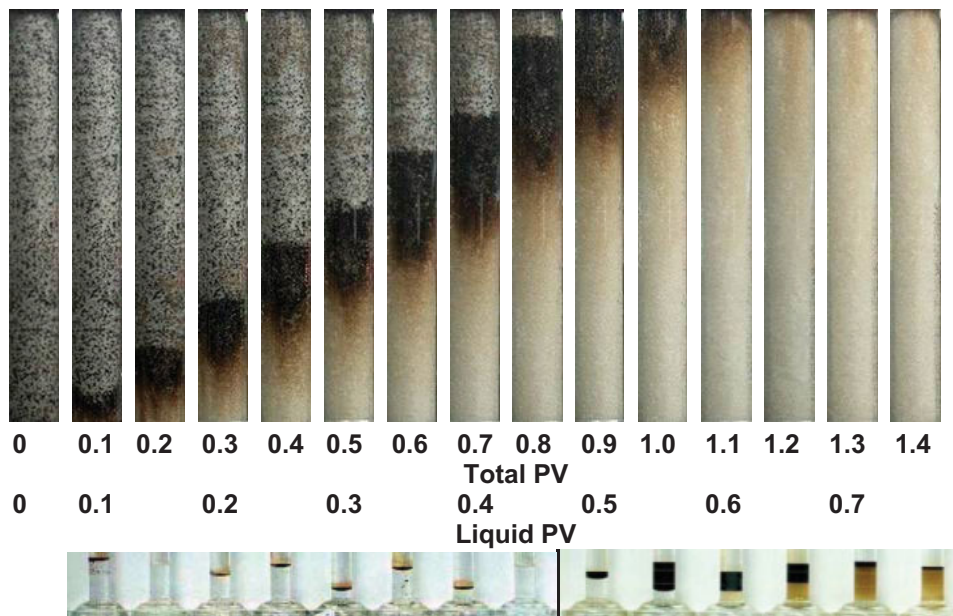


Fig. 9—Displacement profiles and pictures of effluent for the displacement of SMY residual crude oil by ASPF with constant-pressure injection.

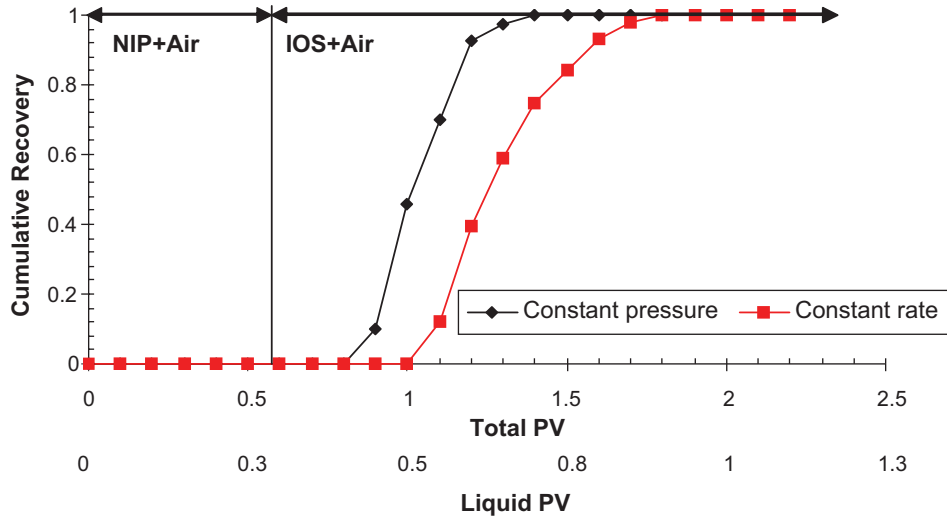


Fig. 10—Recovery of SMY residual oil with ASPF, comparing constant pressure (1.2 psi/ft) and constant rate (20 ft/D).

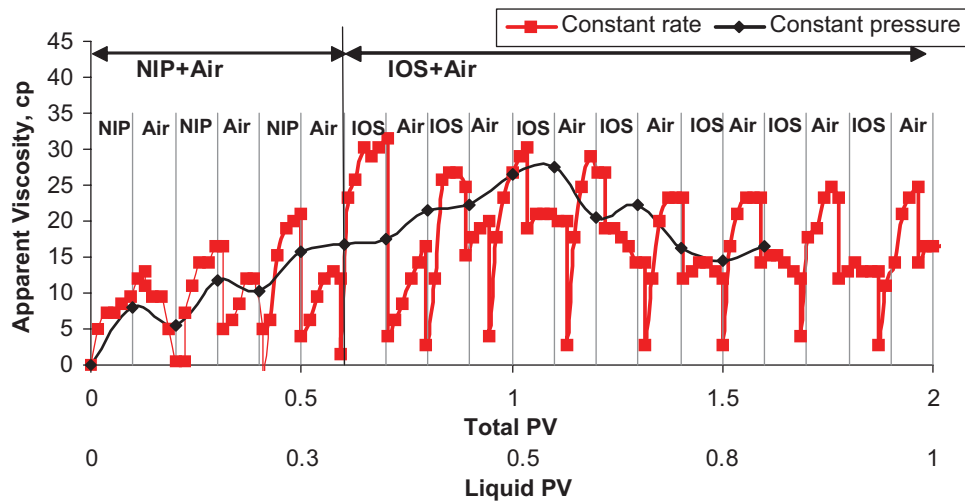


Fig. 11—Apparent viscosity of ASPF displacing SMY crude oil, comparing constant pressure (1.2 psi/ft) and constant rate (20 ft/D). Apparent viscosity for the constant-pressure injection had only one data point at the end of each fluid slug injection because only one averaged flow rate was measured during each slug injection.

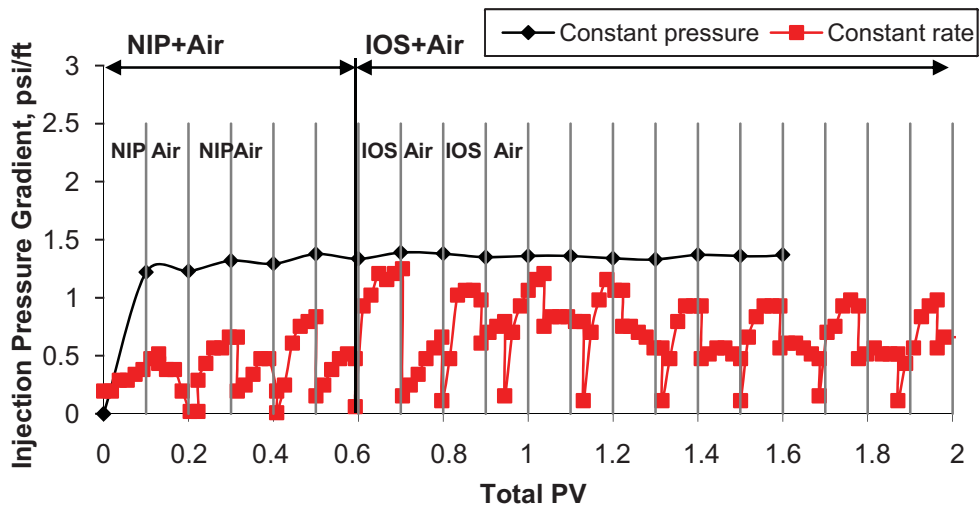


Fig. 12—Pressure history of ASPF displacing SMY crude oil, comparing constant pressure (1.2 psi/ft) and constant rate (20 ft/D).

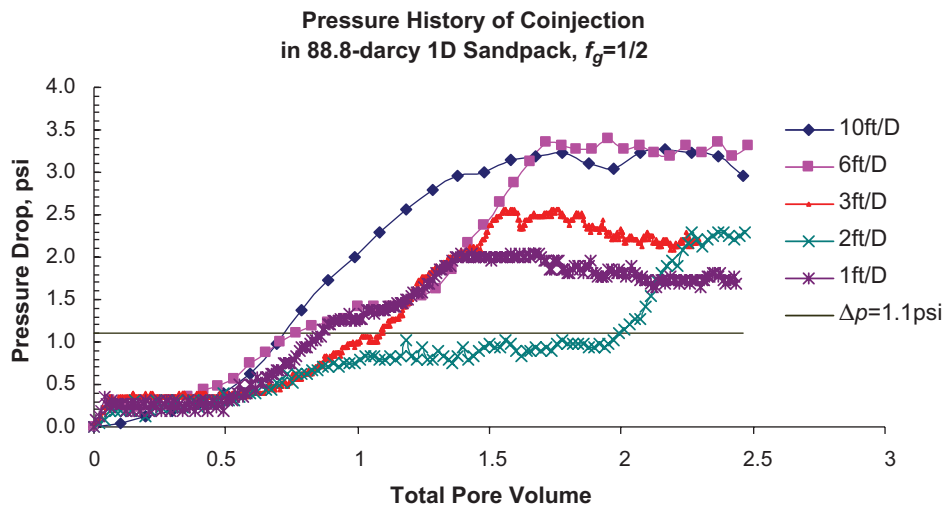


Fig. 13—Pressure history during surfactant/air coinjection in a 88.8-darcy 1D sandpack, $f_g = \frac{1}{2}$, $\nabla p^* = 1.1$ psi/ft. Surfactant was 0.2% AOS 16-18 in 2% NaCl and 1% Na_2CO_3 .

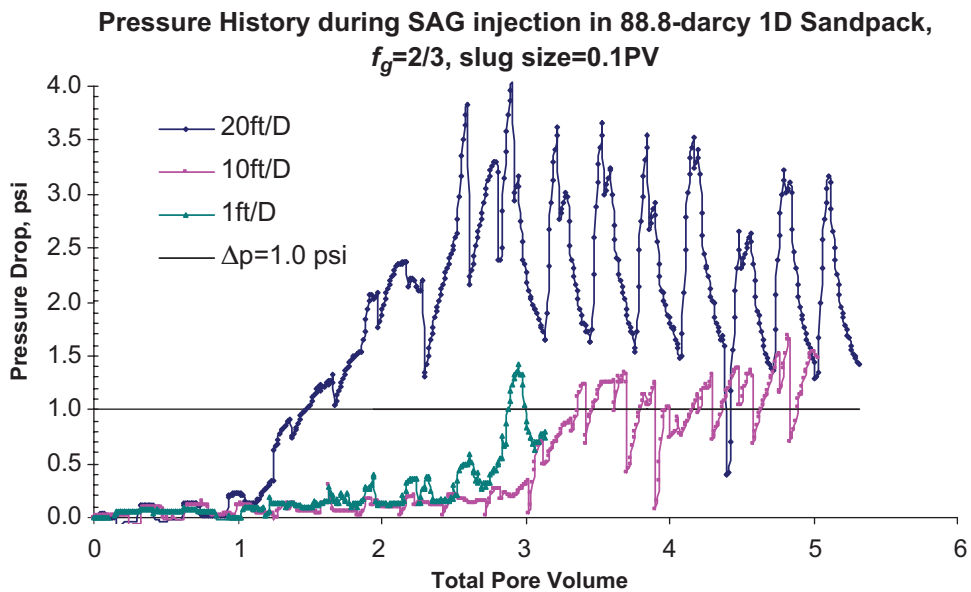


Fig. 14—Pressure history during SAG injection in a 88.8-darcy 1D sandpack, $f_g = \frac{2}{3}$, slug size = 0.1 PV, $\nabla p^* = 1.0$ psi/ft. Surfactant was 0.2% AOS 16-18 in 2% NaCl and 1% Na_2CO_3 .

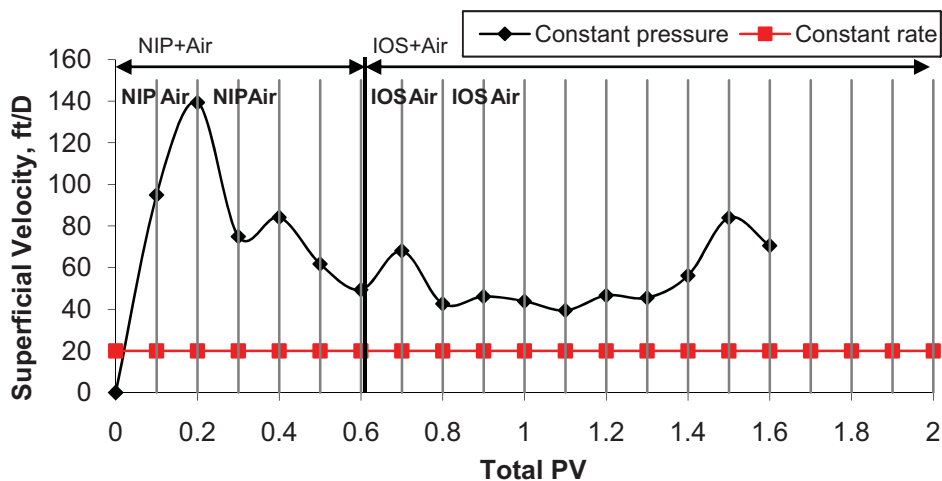


Fig. 15—Injection rate during ASPF displacing SMY crude oil, comparing constant pressure (1.2 psi/ft) and constant rate (20 ft/D).

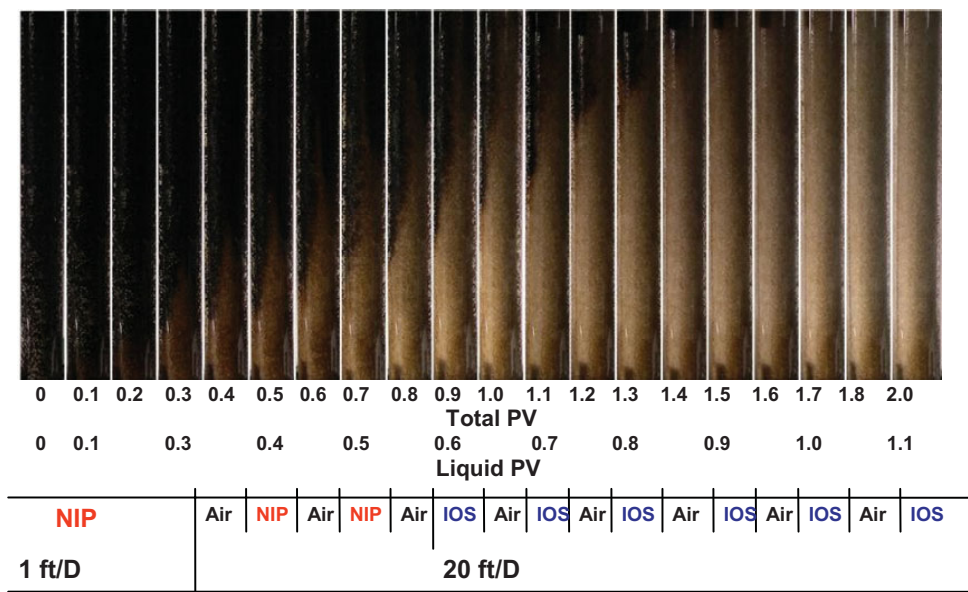


Fig. 16—Profiles of the displacement of 266-cp Crude B with ASP and ASPF.

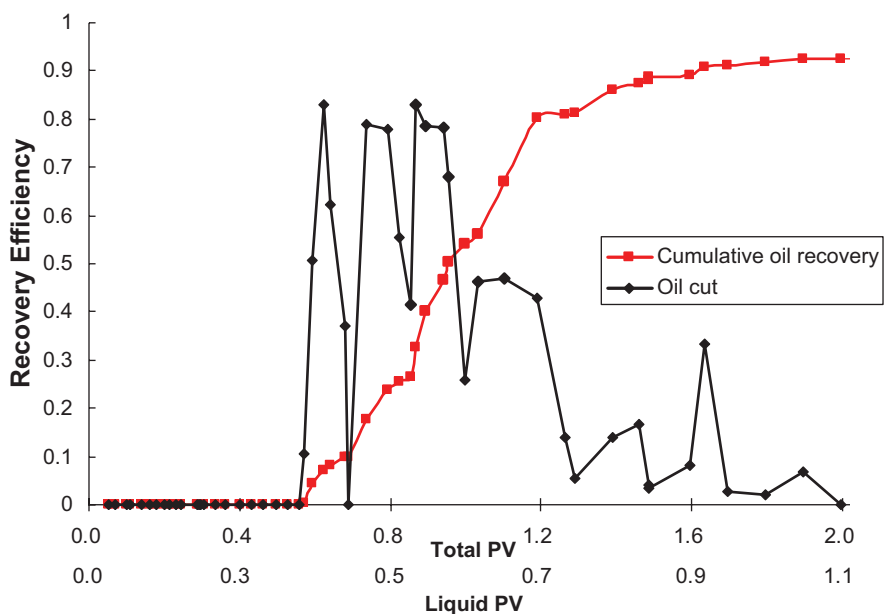


Fig. 17—Recovery of waterflood remaining oil, 266-cp Crude B with ASP and ASPF. Oil cut was the volume fraction of oil in the liquid effluent after each slug injection.

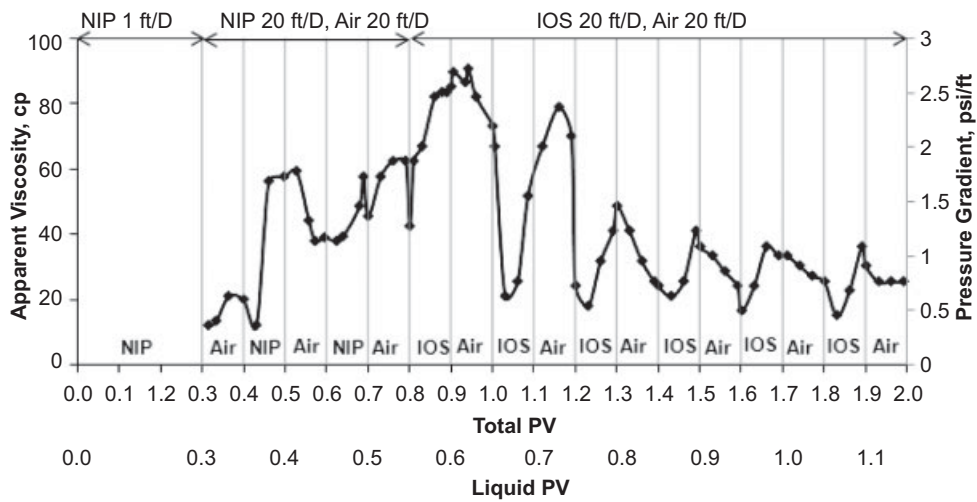


Fig. 18—Apparent viscosity and pressure gradient of ASPF for Crude B. During first 0.3 PV of NIP injection, because of very low rate and very high permeability, pressure was too low to be measured accurately.

to the oil. The displacement profiles shown in Fig. 16 (and visual observations) showed very little change in saturation during the ASP injection. Movement of oil became visible immediately upon injection of air. Oil breakthrough occurred at 0.6 TPV. The early oil production consisted of water-in-oil emulsion and free gas. Later, the oil was produced as oil-in-water emulsion and gas bubbles (foam). Emulsified oil was observed from effluent. Visual observation of the sandpack showed very little movement of oil during liquid injection, but the oil appeared to move with passage of gas bubbles. The oil cut and apparent viscosity showed large changes as slugs of liquid and gas were alternated (Figs. 17 and 18, respectively). A remarkable observation is that foam injection started at 0.3 PV and most of the oil was displaced by 1.3 TPV; almost-piston-like displacement was observed during foam injection.

It appears that foam had a greater role than just mobility control. We speculate that as gas/water interfaces advance through pore throats, the local capillary number (and pressure gradient) become large enough to displace oil/water interfaces also through neighboring pore throats and, thus, emulsify oil. This appears likely because the oil/water IFT is several orders of magnitude less than the gas/water surface tension. The gas bubbles thus displaced the viscous oil through attrition and dispersion as oil-in-water emulsion. The low IFT minimized trapping of oil during emulsion flow. This speculation is consistent with the observation that the apparent viscosity in Fig. 18 is far less than the oil viscosity of 266 cp. Observation from glass micromodel studies of displacement mechanism with NI blend and Crude B showed that oil was emulsified and flowed as oil-in-water emulsion phase. Later, when air was injected, oil drops tended to adhere to the liquid/gas

interface. When this interface was advanced as gas flowed, the oil drops were mobilized at the same rate. The presence of high oil saturation destabilizes foam, and the pressure gradient is focused at fewer advancing gas/water interfaces. A region where oil saturation is low has stable foam and its resistance diverts the injected fluids to regions of high oil saturation.

Mobility Control in Heterogeneous 2D Sandpack. The effect of mobility control is most apparent in the sweep of layered, heterogeneous systems. The sweep of dyed water with water only, water alternating with gas (WAG), and SAG was evaluated in the 2D sandpack (Fig. 1).

The sandpack was initially saturated with green-dyed water. The WAG and SAG processes were injected with slugs of liquid alternating with slugs of air. The size of the smaller slug was 0.1 PV. Fluid was distributed between three inlets through a manifold (Fig. 1). Injection was conducted with a specified injection pressure.

Photographs of the sandpack were taken at the end of each fluid injection. Each photograph was converted to a binary image (green and nongreen). The sweep efficiency is the fraction of the area that is nongreen.

Sweep With Water or WAG. Sweep of the layered sandpack with water only or WAG is compared in Fig. 19. The upper, high-permeability layer was quickly swept in either water only or WAG injection. However, multiple PV injections were required to sweep the lower-permeability layer. The injection volume is expressed as total fluid (liquid plus gas). Inspection shows that sweep of the lower-permeability layer is a function only of the liquid volume (i.e., independent of the volume of gas injected). This can be seen

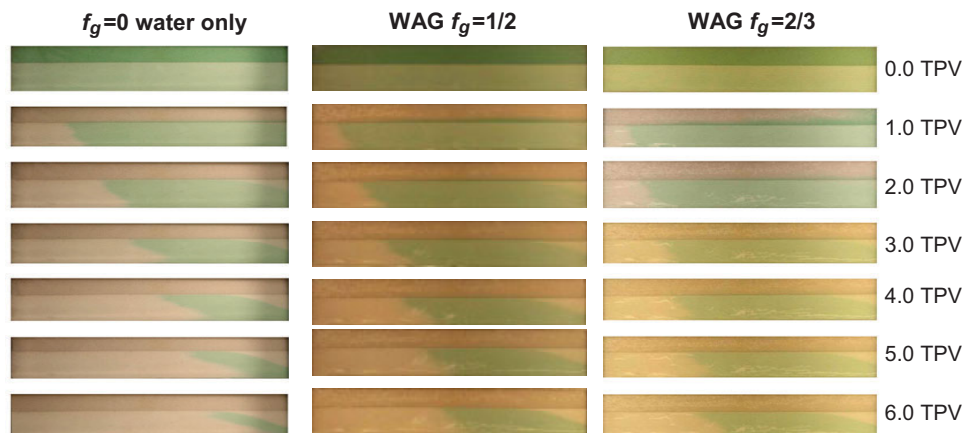


Fig. 19—Profiles of sweep with waterflood or WAG in sandpack with 19:1 permeability ratio.

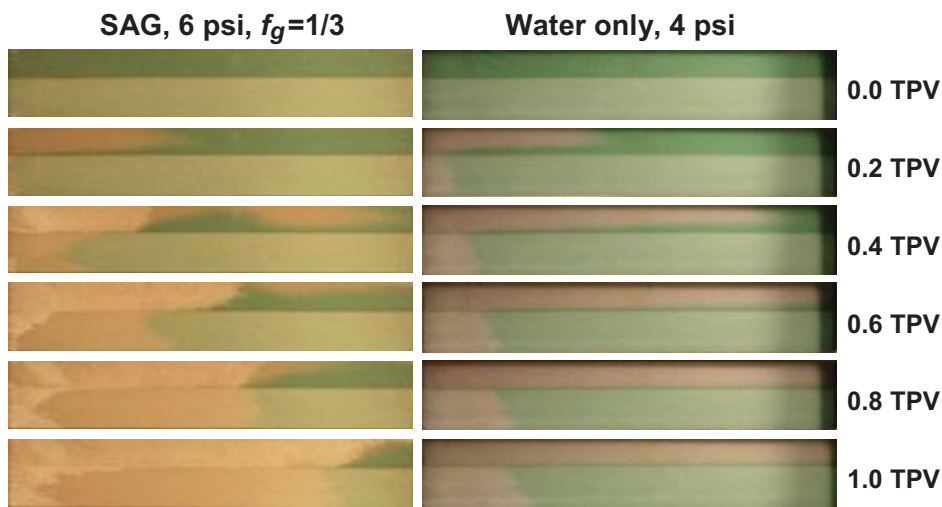


Fig. 20—Comparison of SAG with waterflood in sandpack with 19:1 permeability ratio.

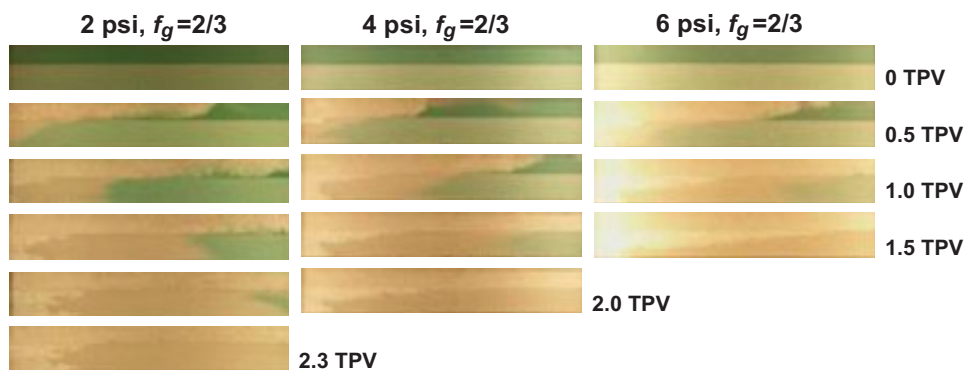


Fig. 21—SAG injection at 2, 4, and 6 psi with $f_g = 2/3$. Injection at 8 psi did not differ much from 6 psi. Bottom photo in each column indicates 100% sweep efficiency.

by comparing the sweep at 2, 4, and 6 TPV in Fig. 19 for water only, gas fraction $f_g = 1/2$, and $f_g = 2/3$, respectively.

Foam Mobility Control. Sweep with SAG is compared with water only in Fig. 20. The surfactant solution was 0.2% AOS 16-18 in 1% Na_2CO_3 and 2% NaCl. The sandpack was completely swept with 1.3 TPV with the SAG process at $f_g = 1/3$ and 6-psi injection pressure. By comparison, the lower-permeability layer was only one-third swept with water at the same injection volume.

Sweep with SAG of different injection pressures is compared in Fig. 21. Sweep improved with increase in injection pressure from 2 to 6 psi. There was very little improvement with changing injection pressure to 8 psi. This is consistent with the interpretation that a critical pressure gradient must be exceeded to generate strong foam by bubble division.

Sweep of SAG with different gas fractions at 6-psi injection pressure is compared in Fig. 22. To achieve 100% sweep efficiency

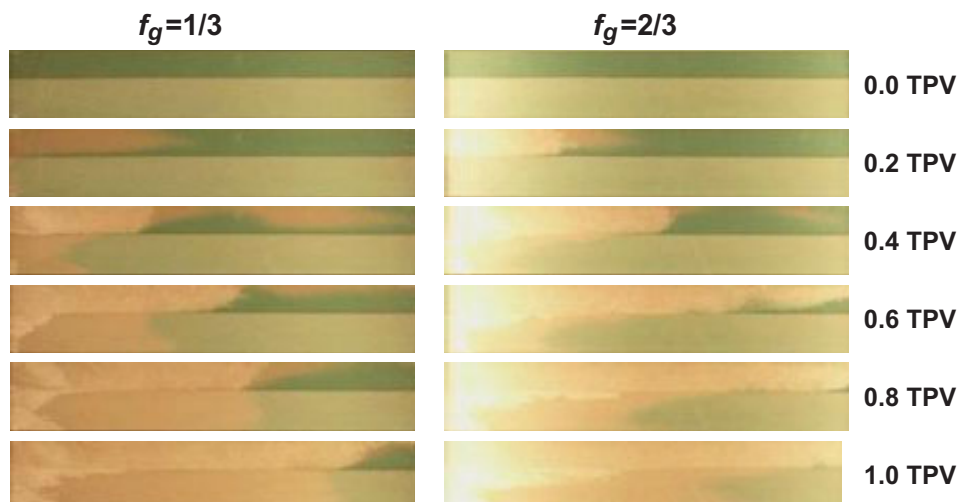


Fig. 22—Comparison of SAG with $f_g = 1/3$ and $2/3$ for 6-psi injection pressure.

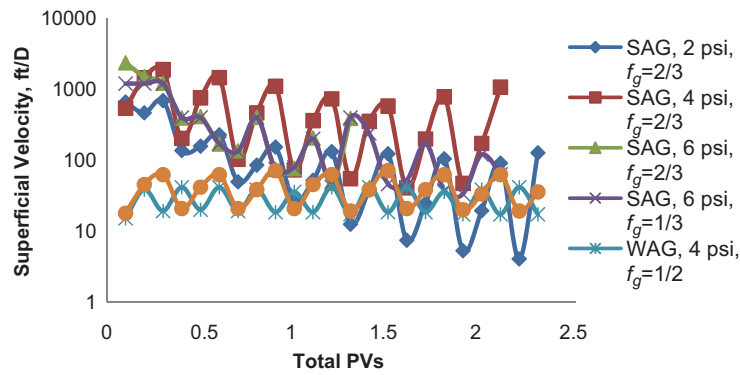


Fig. 23—Flow rates during SAG and WAG injection at constant pressure.

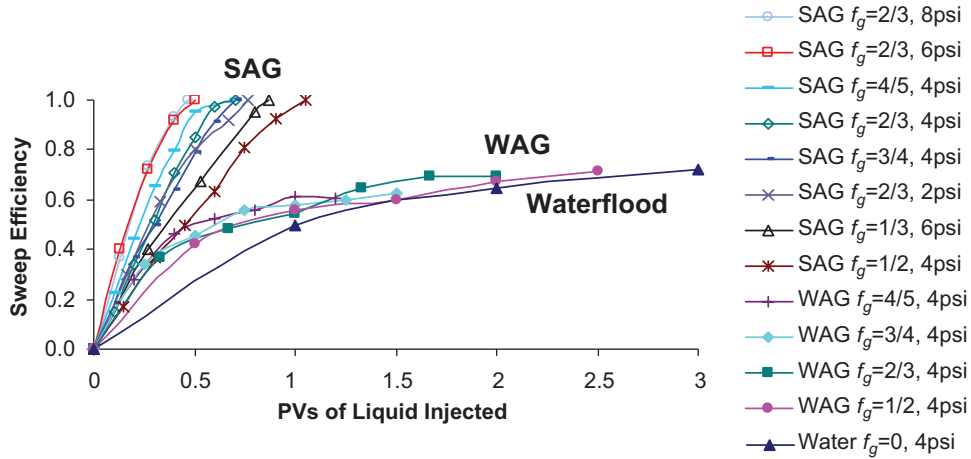


Fig. 24—Sweep in sandpack with 19:1 permeability contrast, SAG, WAG, and waterflood.

required 1.3 and 1.5 TPV for $f_g = 1/3$ and $2/3$, respectively. Expressed as liquid volume, 0.87 and 0.5 liquid PV (LPV), respectively, were required.

Flow rates during WAG and SAG injection are compared in Fig. 23. The overall decreasing trend in the SAG injection rates indicates that foam reduced mobility more effectively than WAG.

Summary of Sweep Efficiency. The sweep efficiency of all experiments is summarized in Fig. 24. Here, sweep is expressed as a function of liquid volume injected because, with this group, waterflood and WAG showed the same performance, as indicated

earlier. SAG clearly has better sweep efficiency in this system, with a 19:1 permeability contrast.

Description of Crossflow. Crossflow between the two layers had an important role in improving sweep efficiency with foam. Two types of crossflow were identified, as illustrated in Fig. 25. The first type of crossflow occurred behind the foam front in the high-permeability layer, diverting surfactant solution into the low-permeability layer (Fig. 26). The second type of crossflow occurred from the low-permeability layer to the high-permeability layer, ahead of the foam front (Fig. 27).

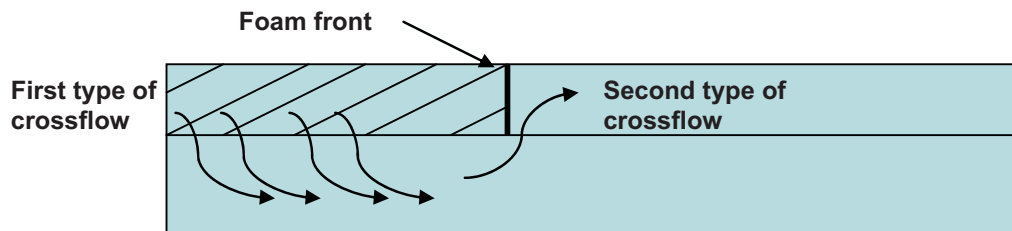


Fig. 25—Schematic illustrating two types of crossflow during foam flooding.



Fig. 26—Example of diversion by crossflow of liquid (colorless) behind foam front in high-permeability layer to the low-permeability layer. 0.8-TPV SAG with $f_g = 1/3$, 6-psi injection pressure.



Fig. 27—Example of crossflow of the second type: crossflow of green-dyed liquid from low-permeability layer to high-permeability layer ahead of the foam bank. 0.4 TPV, $f_g = 1/3$, 6-psi injection pressure.

The diversion of liquid from foam in the high-permeability layer to the low-permeability layer is an important attribute of foam and requires further study. After the green-dyed water was completely swept out of the sandpack at 1.3 TPV ($f_g = 1/3$ experiment in Fig. 20), the experiment was continued by injecting green-dyed surfactant slugs alternating with gas, as shown in Fig. 28. At 1.3 TPV, foam had entered only approximately 15% of the low-permeability layer. At 1.5 TPV, the green color was apparent in the high-permeability layer and near the layer boundary in the low-permeability layer. Subsequent photos show the green-dyed surfactant solution progressively sweeping out the low-permeability layer by the end of 2.1 TPV. Recall that the waterflood in Fig. 19 had not completely swept out the low-permeability layer after 6 PV.

The crossflow mentioned here is a recognized attribute of favorable mobility ratio displacement in layered systems (Zapata and Lake 1981). However, with foam flow, the fluid that was diverted into the low-permeability layer was primarily the liquid component of foam. With a polymer or ASPF, viscous polymer solution would be diverted into the low-permeability layer.

Distribution of Produced Liquid. The distribution of produced liquid between the two layers was measured to interpret the mechanisms for the improved sweep with foam. Fig. 29 shows the liquid produced from the upper (high-permeability) and the lower (low-permeability) layer during $f_g = 1/3$ SAG injection at 20 ft/D after foam had been well established in the high-permeability layer. The production from individual layers was measured from the produced fluids from the top and bottom flow lines in Fig. 1. Fig. 29 shows

that nearly all of the liquid was produced from the low-permeability layer. During periods of gas injection, foam was produced from the high-permeability layer, but flow from the high-permeability layer stopped during liquid injection. Thus, foam was successful in diverting nearly all of the liquid to the low-permeability layer, even though the permeability contrast was 19:1.

Apparent Viscosity With Foam. Pressure-drop and flow-rate data were used to compute the apparent viscosity during the SAG experiment with $f_g = 1/3$, 0.2 PV of surfactant, and 0.1-PV gas injection. Figs. 30 and 31 are plots of the apparent viscosity computed for flow at constant pressure and constant velocity, respectively. The overall permeability was used to compute apparent viscosity.

Fig. 30 shows the apparent viscosity increasing gradually with continued SAG injection. The sandpack was initially filled with water (1 cp). SAG injection at 6 psi (3.6 psi/ft) was greater than the critical pressure gradient required for strong foam of approximately 1.5 psi/ft. The slow increase in apparent viscosity was not because of lack of generation of foam (see Fig. 20). Apparently, the preferential flow of gas in the high-permeability layer and diversion of liquid to the low-permeability layer redistributed the flow so as to have lower apparent viscosity than in the 1D experiments discussed earlier (Figs. 6, 11, and 18). This is consistent with observations of foam flow in three dimensions (Li et al. 2006).

The apparent viscosity with constant pressure and constant rate are compared with Figs. 30 and 31, respectively. It is remarkable that SAG injection at 6 psi had apparent viscosity increasing during gas

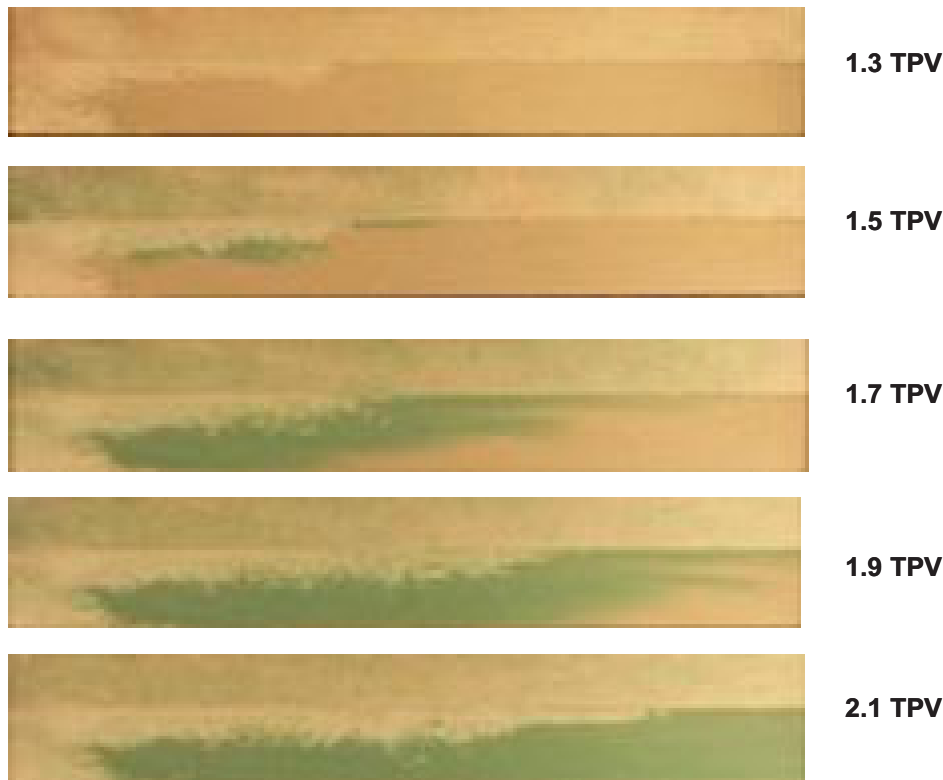


Fig. 28—Diversion of green-dyed surfactant solution from high-permeability to low-permeability layer.

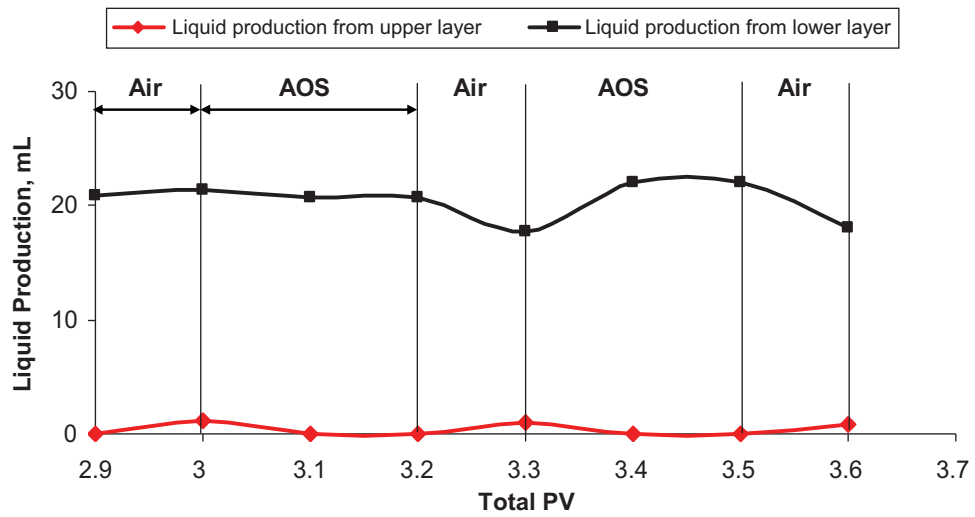


Fig. 29—Liquid production from the upper and lower layers.

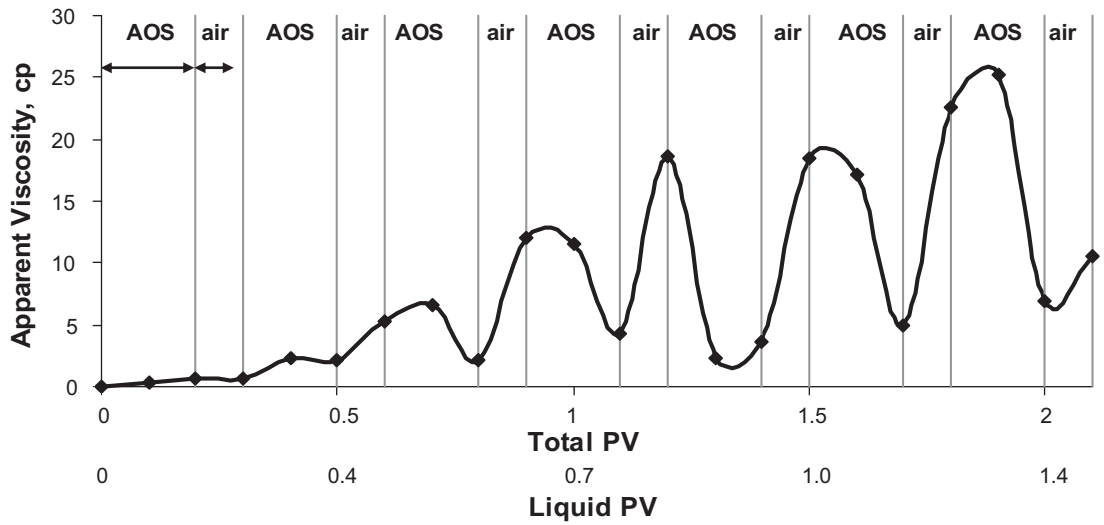


Fig. 30—Apparent viscosity during SAG injection at 6 psi.

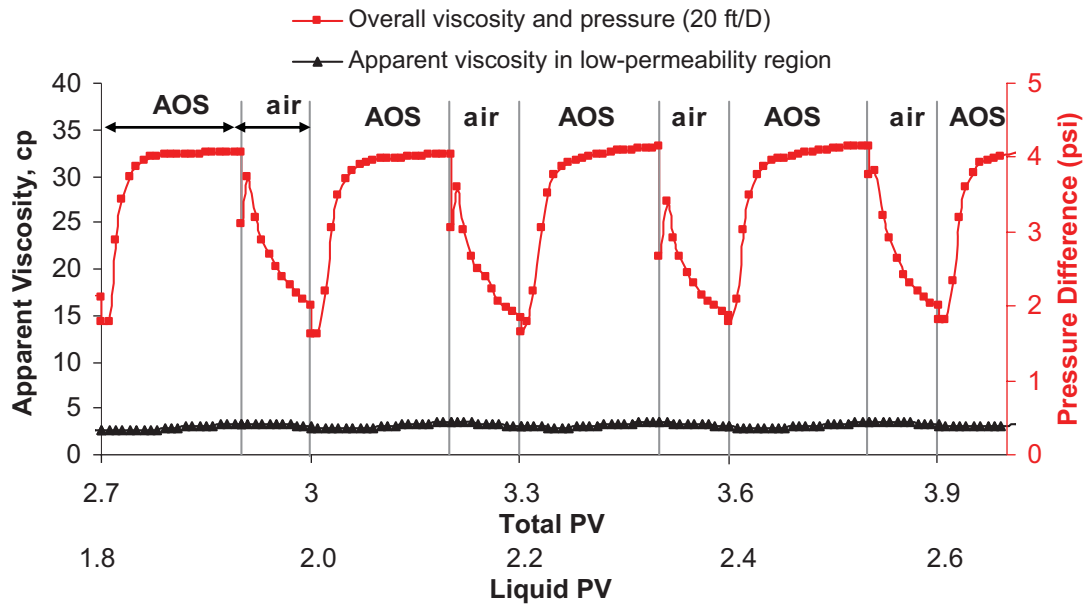


Fig. 31—Apparent viscosity during SAG injection at 20 ft/D.

injection and decreasing during surfactant injection while the constant-rate experiment (at lower pressures) had the opposite trend.

It was mentioned earlier that only liquid was produced from the low-permeability layer. The apparent viscosity for flow in the low-permeability layer was computed using the flow from that layer, pressure drop across the internal pressure taps, and the permeability of the low-permeability layer. The apparent viscosity in the low-permeability was only slightly greater than that of water. Thus, a combination of flow redistribution and permeability dependence of apparent viscosity compensates for the 19:1 permeability contrast.

Conclusions

- A foam drive with surfactant SAG can be used as an alternative for polymer drive in ASP EOR.
- The apparent viscosity of SAG is a function of pressure gradient, permeability, and gas fraction.
- A moderately viscous (266-cp) oil was displaced successfully with ASP and SAG. The apparent viscosity of the displacement process was much less than that of the crude oil. The oil may have been dispersed by the foam as oil-in-water emulsion.
- The vertical sweep of a layered sandpack with a 19:1 permeability contrast was greatly enhanced with SAG compared to waterflood or WAG.
- Crossflow results from the favorable-mobility-ratio displacement, but the fluid that is diverted to the low-permeability layer is primarily the liquid fraction of the foam.

Acknowledgment

The financial support of US Department of Energy Grant DE-FC26-03NT15406 and the member companies of the Rice University Consortium on Processes in Porous Media is gratefully acknowledged. The member companies are Anadarko, Baker Hughes, Chevron, ConocoPhillips, Core Labs, ExxonMobil, Marathon, Oil Chem, PTS, Schlumberger, Shell, Saudi Aramco, and Total. Shell is acknowledged for donation of the 2D sandpack.

References

- Bertin, H.J., Apaydin, O.G., Castanier, L.M., and Kovscek, A.R. 1999. Foam Flow in Heterogeneous Porous Media: Effect of Cross Flow. *SPE J.* **4** (2): 75–82. SPE-56009-PA. doi: 10.2118/56009-PA.
- Blaker, T., Aarra, M.G., Skauge, A., Rasmussen, L., Celius, H., Martinsen, H.A., and Vassenden, F. 2002. Foam for Gas Mobility Control in the Snorre Field: The FAWAG Project. *SPE Res Eval & Eng* **5** (4): 317–323. SPE-78824-PA. doi: 10.2118/78824-PA.
- Falls, A.H., Hirasaki, G.J., Patzek, T.W., Gauglitz, P.A., Miller, D.D., and Ratulowski, J. 1988. Development of a Mechanistic Foam Simulator: The Population Balance and Generation by Snap-Off. *SPE Res Eng* **3** (3): 884–892. SPE-14961-PA. doi: 10.2118/14961-PA.
- Garrett, P.R. ed. 1992. *Defoaming: Theory and Industrial Applications*, Vol. 45. Boca Raton, Florida: Surfactant Science Series, CRC Press.
- Gauglitz, P.A., Friedmann, F., Kam, S.I., and Rossen, W.R. 2002. Foam generation in homogeneous porous media. *Chemical Engineering Science* **57** (19): 4037–4052. doi: 10.1016/S0009-2509(02)00340-8.
- Gdansk, R.D. 1993. Experience and Research Show Best Designs for Foam-Diverted Acidizing. *Oil & Gas Journal* **91** (36): 85–89.
- Heller, J.P. 1994. CO₂ Foam in Enhanced Oil Recovery. In *Foams: Fundamentals and Applications in the Petroleum Industry*, ed. L.L. Schramm, No. 242, 201–234. Washington, DC: Advances in Chemistry Series, American Chemical Society.
- Hirasaki, G.J. 1989. The Steam-Foam Process. *J Pet Technol* **41** (5): 449–456. SPE-19505-PA. doi: 10.2118/19505-PA.
- Hirasaki, G.J., Jackson, R.E., Jin, M., Lawson, J.B., Londergan, J., Meinardus, H., Miller, C.A. et al. 2000. Field Demonstration of the Surfactant/Foam Process for Remediation of a Heterogeneous Aquifer Contaminated with DNAPL. In *NAPL Removal: Surfactants, Foams, and Microemulsions*, ed. S. Fiorenza, C.A. Miller, C.L. Oubre, and C.H. Ward, Part 1, 3–163. AATDF monograph series, Boca Raton, Florida, USA: Lewis Publishers, CRC Press.
- Hirasaki, G.J., Miller, C.A., Szafranski, R., Tanzil, D., Lawson, J.B., Meinardus, H., Jin, M., Londergan, J.T., Jackson, R.E., Pope, G.A., and Wade, W.H. 1997. Field Demonstration of the Surfactant/Foam Process for Aquifer Remediation. SPE 39292 prepared for presentation at the SPE Annual Technical Conference and Exhibition, San Antonio, Texas, USA, 5–8 October. doi: 10.2118/39292-MS.
- Kam, S.I. and Rossen, W.R. 2003. A Model for Foam Generation in Homogeneous Porous Media. *SPE J.* **8** (4): 417–425. SPE-87334-PA. doi: 10.2118/87334-PA.
- Khatib, Z.I., Hirasaki, G.J., and Falls, A.H. 1988. Effects of Capillary Pressure on Coalescence and Phase Mobilities in Foams Flowing Through Porous Media. *SPE Res Eng* **3** (3): 919–926. SPE-15442-PA. doi: 10.2118/15442-PA.
- Kovscek, A.R. and Bertin, H.J. 2002. Estimation of Foam Mobility in Heterogeneous Porous Media. Paper SPE 75181 presented at the SPE/DOE Improved Oil Recovery Symposium, Tulsa, 13–17 April. doi: 10.2118/75181-MS.
- Lau, H.C. and O'Brien, S.M. 1988. Effects of Spreading and Non-spreading Oils on Foam Propagation through Porous Media. *SPE Res Eng* **3** (3): 893–896. SPE-15668-PA. doi: 10.2118/15668-PA.
- Lawson, J.B. and Reisberg, J. 1980. Alternate Slugs of Gas and Dilute Surfactant for Mobility Control During Chemical Flooding. Paper SPE 8839 presented at the SPE/DOE Enhanced Oil Recovery Symposium, Tulsa, 20–23 April. doi: 10.2118/8839-MS.
- Li, B., Hirasaki, G.J., and Miller, C.A. 2006. Upscaling of Foam Mobility Control to Three Dimensions. Paper SPE 99719 presented at the SPE Symposium on Improved Oil Recovery, Tulsa, 26–29 April. doi: 10.2118/99719-MS.
- Liu, S., Li, R.F., Miller, C.A., and Hirasaki, G.J. 2008a. ASP Processes: Wide Range of Conditions for Good Recovery. Paper SPE 113936 presented at the SPE/DOE Symposium on Improved Oil Recovery, Tulsa, 19–23 April. doi: 10.2118/113936-MS.
- Liu, S., Zhang, D.L., Yan, W., Puerto, M., Hirasaki, G.J., and Miller, C.A. 2008b. Favorable Attributes of Alkali-Surfactant-Polymer Flooding. *SPE J.* **13** (1): 5–16. SPE-99744-PA. doi: 10.2118/99744-PA.
- Manlowe, D.J., and Radke, C.J. 1990. A Pore-Level Investigation of Foam/Oil Interactions in Porous Media. *SPE Res Eng* **5** (4): 495–502. SPE-18069-PA. doi: 10.2118/18069-PA.
- Nguyen, Q.P., Currie, P.K., and Zitha, P.L.J. 2005. Effect of Capillary Cross-Flow on Foam-Induced Diversion in Layered Formations. *SPE J.* **10** (1): 54–65. SPE-82270-PA. doi: 10.2118/82270-PA.
- Nikolov, A.D., Wasan, D.T., Huang, D.W., and Edwards, D.A. 1986. The Effect of Oil on Foam Stability: Mechanisms and Implications for Oil Displacement by Foam in Porous Media. Paper SPE 15443 presented at the SPE Annual Technical Conference and Exhibition, New Orleans, 5–8 October. doi: 10.2118/15443-MS.
- Osterloh, W.T. and Jante, M.J. Jr. 1992. Effects of Gas and Liquid Velocity on Steady-State Foam Flow at High Temperature. Paper SPE 24179 presented at the SPE/DOE Enhanced Oil Recovery Symposium, Tulsa, 22–24 April. doi: 10.2118/24179-MS.
- Patzek, T.W. 1996. Field Applications of Steam Foam for Mobility Improvement and Profile Control. *SPE Res Eng* **11** (2): 79–86. SPE-29612-PA. doi: 10.2118/29612-PA.
- Rossen, W.R. 1996. Foams in Enhanced Oil Recovery. In *Foams: Theory, Measurements and Applications*, ed. R.K. Prud'Homme and S. Khan, 413–464. New York: Marcel Dekker.
- Rossen, W.R. and Bruining, J. 2007. Foam Displacements With Multiple Steady States. *SPE J.* **12** (1): 5–18. SPE-89397-PA. doi: 10.2118/89397-PA.
- Tanzil, D., Hirasaki, G.J., and Miller, C.A. 2002a. Mobility of Foam in Heterogeneous Media: Flow Parallel and Perpendicular to Stratification. *SPE J.* **7** (2): 203–212. SPE-78601-PA. doi: 10.2118/78601-PA.
- Tanzil, D., Hirasaki, G.J., and Miller, C.A. 2002b. Conditions for Foam Generation in Homogeneous Porous Media. Paper SPE 75176 presented at the SPE/DOE Improved Oil Recovery Symposium, Tulsa, 13–17 April. doi: 10.2118/75176-MS.
- Wang, D., Cheng, J., Yang, Z., Li, Q., Wu, W., and Yu, H. 2001. Successful Field Test of the First Ultra-Low Interfacial Tension Foam Flood. Paper SPE 72147 presented at the SPE Asia Pacific Improved Oil Recovery Conference, Kuala Lumpur, 6–9 October. doi: 10.2118/72147-MS.
- Yan, W., Miller, C.A., and Hirasaki, G.J. 2006. Foam sweep in fractures for enhanced oil recovery. *Colloids and Surfaces A: Physicochem. Eng. Aspects* **282–283**: 348–359. doi: 10.1016/j.colsurfa.2006.02.067.

- Zapata, V.J. and Lake, L.W. 1981. A Theoretical Analysis of Viscous Crossflow. Paper SPE 10111 presented at the SPE Annual Technical Conference and Exhibition, San Antonio, Texas, USA, 5–7 October. doi: 10.2118/10111-MS.
- Zhang, Y., Yue, X., Dong, J., and Liu, Y. 2000. New and Effective Foam Flooding To Recover Oil in Heterogeneous Reservoir. Paper SPE 59367 presented at the SPE/DOE Improved Oil Recovery Symposium, Tulsa, 3–5 April. doi: 10.2118/59367-MS.
- Zhou, Z.H. and Rossen, W.R. 1994. Applying Fractional-Flow Theory to Foams for Diversion in Matrix Acidization. *SPE Prod & Fac* 9 (1): 29–35; *Trans.*, AIME, 297. SPE-24660-PA. doi: 10.2118/24660-PA.

Robert Feng Li is a graduate student and PhD candidate in the Chemical and Biomolecular Engineering department at Rice University. His thesis advisors are Prof. George J. Hirasaki, and Prof. Clarence A. Miller. His research topic is surfactant EOR and foam mobility control. He holds a BS degree from Zhejiang University, China. **Wei Yan** is a process engineer with IPSI in Houston. He holds a BS degree in chemical engineering from Tianjin University in China and a PhD degree in chemical engineering from Rice University. **Shunhua Liu** holds BS and MS degrees from Tsinghua University, China, both in chemical engineering, and a PhD degree in chemical engineering from Rice University. He joined Occidental Oil and Gas in 2007 as a reservoir engineer in Houston. His areas of expertise are surfactant science, enhanced oil recovery, and numerical

simulation. **George J. Hirasaki** holds a BS degree in chemical engineering from Lamar University and a PhD degree in chemical engineering from Rice University. He had a 26-year career with Shell Development and Shell Oil Companies before joining the Chemical Engineering faculty at Rice University in 1993. At Shell, his research areas were reservoir simulation, EOR, and formation evaluation. At Rice, his research interests are in nuclear magnetic resonance well logging, reservoir wettability, surfactant-enhanced oil recovery, foam mobility control, gas hydrate recovery, asphaltene deposition, and emulsion separation. He received the SPE Lester Uren Award in 1989 and was named an Improved Oil Recovery Pioneer at the 1998 SPE/DOR IOR Symposium. Hirasaki was the 1999 recipient of the Society of Core Analysts Technical Achievement Award. He is a member of the National Academy of Engineers. **Clarence A. Miller** is the Louis Calder Professor Emeritus of Chemical and Biomolecular Engineering at Rice University and a former chairman of the department. He holds BS and PhD degrees from Rice and the University of Minnesota, respectively, both in chemical engineering. Before coming to Rice, Miller taught at Carnegie-Mellon University. He has been a Visiting Scholar at Cambridge University, the University of Bayreuth in Germany, and Delft University of Technology in The Netherlands. His research interests center on emulsions, microemulsions, and foams and their applications in detergency, enhanced oil recovery, and aquifer remediation. He is a coauthor of the book *Interfacial Phenomena*, now in its second edition.